Collision-Induced Dissociation of HS⁻(HCN): Unsymmetrical Hydrogen Bonding in a Proton-Bound Dimer Anion†

F. Ahu Akin and Kent M. Ervin*

Department of Chemistry and Chemical Physics Program, University of Nevada, Reno,
1664 N. Virginia Street, Reno, Nevada 89557

The energy-resolved competitive collision-induced dissociation of the proton-bound complex [HS·H·CN]⁻ is studied in a guided ion beam tandem mass spectrometer. H_2S and HCN have nearly identical gas-phase acidities, and therefore, the HS⁻ + HCN and the CN⁻ + H_2S product channels exhibit nearly the same threshold energies, as expected. However, the HS⁻ + HCN channel has a cross section up to a factor of 50 larger than CN⁻ + H_2S at higher energies. The cross sections are modeled using RRKM theory and phase space theory. The complex dissociates to HS⁻ + HCN via a loose transition state, and it dissociates to CN⁻ + H_2S via a tight transition state. Theoretical calculations show that the proton-transfer potential energy surface has a single minimum and that the hydrogen bonding in the complex is strongly unsymmetrical, with an ion−molecule complex of the form HS⁻··HCN rather than CN⁻··H_2S or an intermediate structure. The requirement for proton transfer before dissociation and curvature along the reaction path impedes the CN⁻ + H_2S product channel.

Introduction

Competitive threshold collision-induced dissociation (TCID) has been applied to a broad range of chemical systems to measure ion complex dissociation energies and relative ion affinities.[1−8] Competitive TCID on proton-bound complexes allows a direct measurement of the gas-phase acidity of an unknown acid relative to a species with well-known acidity.[3−5] In this application, a proton-bound complex, $[A_1HA_2]^-$, is collisionally excited at controlled translational energies and it dissociates into two competitive channels as in eq 1:

$$[A_1HA_2]^- + Xe \rightarrow A_1^- + HA_2 + Xe \qquad (1a)$$

$$\rightarrow A_2^- + HA_1 + Xe \qquad (1b)$$
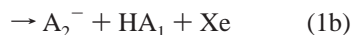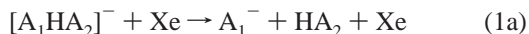
The relative gas-phase acidity, $\delta\Delta_{acid}H_0 = \Delta_{acid}H_0(HA_2) - \Delta_{acid}H_0(HA_1)$, is related to the difference between the two reaction threshold energies, ΔE_0, according to eq 2, provided that there are no reverse activation barriers to dissociation.

$$\delta\Delta_{acid}H_0 = \Delta E_0 = E_0(1b) - E_0(1a) \qquad (2)$$

TCID is performed under nonequilibrium conditions, and therefore, its analysis requires an understanding of the kinetics of the unimolecular dissociation event. Kinetic and competitive shift corrections using statistical rate theory have been incorporated into the data analysis for TCID experiments as described previously.[1,3,9,10] This work examines the modeling of TCID, including a comparison of Rice−Ramsperger−Kassel−Marcus (RRKM) theory[11,12] versus phase space theory (PST)[13,14] and the treatment of the neutral molecular dipole in the long-range potential, for a well-characterized small system where these

effects can be assessed. Specifically, we study competitive TCID for the H_2S/HCN system, eq 3:

$$[HS·H·CN]^- + Xe \rightarrow CN^- + H_2S + Xe \qquad (3a)$$

$$\rightarrow HS^- + HCN + Xe \qquad (3b)$$

$$\rightarrow HS^- + HNC + Xe \qquad (3c)$$

$$\rightarrow HS^-·Xe + HCN \qquad (3d)$$
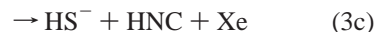
Reactions 3a,b are the primary product channels at low energies. Formation of the HNC isomer channel (eq 3c) is possible at higher energies, and a minor ligand exchange channel, reaction 3d, is observed near threshold. The threshold energy difference, $\Delta E_0 = \delta\Delta_{acid}H_0 = \Delta_{acid}H_0(H_2S) - \Delta_{acid}H_0(HCN)$, corresponds to the 0 K enthalpy of reaction 4.

$$CN^- + H_2S \rightarrow HS^- + HCN \qquad (4)$$
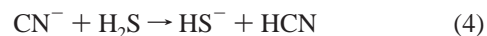
Using literature thermochemistry summarized in Table 1,[15−20] we find $\Delta_rH_0(4) = 2.6 \pm 0.9$ kJ/mol. Because of this small acidity difference, the branching probability between the two dissociation channels in eq 3 will be determined mainly by the sums of states of the transition states for the two channels. H_2S, HCN, and their conjugate bases are well characterized spectroscopically, so the densities of states of the products can be calculated accurately. These conditions allow a good test of the statistical rate models for TCID. The TCID experiments are complemented by electronic structure calculations to obtain structural parameters for the complex and the properties of the potential energy surface for reactions 3 and 4.

Methods

TCID Cross-Section Measurements. Experiments are carried out on our guided ion beam tandem mass spectrometer,

TABLE 1: Literature Thermochemical Values

quantity	value	method
$EA_0(HS)$	$2.314\,338 \pm 0.000\,025$ eV	PD[a]
$D_0(H-SH)$	376.1 ± 0.5 kJ/mol	PTS[b]
$\Delta_{acid}H_0(H_2S)$	1464.92 ± 0.04 kJ/mol	TIPPS[c]
$EA_0(CN)$	3.862 ± 0.004 eV	PES[d]
$D_0(H\text{-}CN)$	522.9 ± 0.8 cm⁻¹	PTS[e]
$\Delta_{acid}H_0(HCN)$	1462.3 ± 0.9 kJ/mol	$D(HA) - EA(A) + IE(H)$[f]
$\Delta_r H_0(4)$	2.6 ± 0.9 kJ/mol	$\Delta_{acid}H_0(H_2S) - \Delta_{acid}H_0(HCN)$
$\Delta_r G_{298}(4)$	6.2 ± 0.9 kJ/mol	g

[a] Photodetachment threshold.[15] [b] Photofragment translational spectroscopy.[18] [c] Threshold ion-pair production spectroscopy.[16] [d] Negative-ion photoelectron spectroscopy.[17] [e] Reference 19. [f] IE(H) = 1312.049 38 ± 0.000 02 kJ/mol.[20] [g] Thermal enthalpy and entropy corrections from statistical mechanics in the rigid-rotor harmonic-oscillator approximation.

which is described in detail elsewhere.[21−23] The [HS··H··CN]⁻ complex is synthesized in the flow tube reactor using a microwave discharge source with helium carrier gas. The CN⁻ ions are produced by passing the vapor from liquid CH₃CN (J.T. Baker, 99.8−100%) at room temperature through the microwave discharge. H₂S gas (Matheson Tri-Gas, 99%) is introduced via a ring inlet downstream of the discharge to react with the CN⁻ ions to produce [HS·H·CN]⁻. As will be shown experimentally and theoretically in this work (vide infra), the [HS·H·CN]⁻ complex actually has the structure HS⁻··HCN; i.e., the CN⁻ + H₂S reaction leads to proton transfer along with complex formation. The HS⁻··HCN complex comprises the major product of the CN⁻ + H₂S reaction in the flow tube under the conditions used, for which the CN⁻ ion is largely depleted by the addition of H₂S. The ions are cooled by about 10^5 collisions in the flow tube at a helium pressure of 0.36 Torr and at room temperature. The complex is expected to be thermalized to 300 K under these reaction conditions. The ions are sampled through a nose cone aperture, focused and accelerated to 1 kV, injected into a magnetic sector momentum analyzer where the HS⁻··HCN ions are mass selected, and then decelerated and injected into an octopole ion guide. The octopole ion guide passes through a collision cell containing Xe with which the HS⁻··HCN ions collide at controlled translational energies. During our cross-section measurements, we observed low-energy axially trapped ions in the octopole ion guide which result in artifact reaction products at collision energies near threshold from multiple collision events, as discussed previously.[21] To avoid this problem, we carried out the ion injection in the pulsed ion beam mode, for which the ions are pulsed by a deflector after the second slit of the magnetic sector and trapped ions are eliminated from the octopole after each cycle.[21] The reactant and product ions are collected and mass analyzed by a quadrupole mass filter and counted by an electron multiplier operated in negative-ion pulse counting mode.

The absolute cross sections are acquired as a function of laboratory ion energy, which is measured using retarding potential analysis[21] and converted to the relative collision energy of the reactants in the center-of-mass (cm) frame.[24] To obtain the absolute cross sections under single-collision conditions, the data are collected at three different gas cell pressures in the range 0.04−0.1 mTorr and the cross sections are extrapolated to zero pressure. The cross sections did not show any significant dependence on Xe pressure in these experiments. Five independent data sets obtained on different days are analyzed individually.

TCID Data Analysis. The energy-dependent cross sections for the two dissociation channels in reaction 3 are fit using the competitive TCID model of Rodgers and Armentrout,[1] which

explicitly treats competitive and kinetic shifts in TCID using RRKM theory.[3,9,11,12] The details of our application of the models have been summarized recently.[5] In this work, we employ phase space theory (PST),[14] which explicitly conserves total angular momentum, in addition to RRKM theory. We use a version of PST with a classical treatment of angular momentum conservation as developed by Bowers, Chesnavich, and their co-workers[14,25−30] The statistical theory rate constant for unimolecular dissociation of the complex to channel j is given by

$$k_j(E^*,J;E_0(j)) = \frac{s_j N_{vrj}^{\ddagger}(E^* - E_0(j),J)}{h\rho_{vr}(E^*,J)} \quad (5)$$

Here E^* is the total internal energy of the energized molecule (EM), $N_{vrj}^{\ddagger}$ is the sum of rovibrational states at the transition state (TS) configuration, $E_0(j)$ is the threshold dissociation energy, ρ_{vr} is the rovibrational density of states of the EM, h is Planck's constant, s_j is the reaction degeneracy, and J is the total angular momentum quantum number. The primary difference between RRKM theory and PST is that for PST the total angular momentum J is explicitly conserved in the calculations of the sum and density of states in eq 5. In the form of RRKM theory used here, angular momentum effects are treated approximately by subtracting the rotational energy of the "inactive" overall rotation of the complex $E_r(J)$ from E^* in the calculation of ρ_{vr} and correspondingly subtracting the rotational energy of the transition state, $E_r^{\ddagger}(J)$, from E^* in the calculation of N_{vr}.[1,9,11,12] Vibrations are treated as Morse oscillators. For the rotational states, nonlinear molecules are treated in the symmetric top approximation with independent one-dimensional and two-dimensional rotational constants. An exception is that in the Bowers−Chesnavich implementation of classical PST used here, nonlinear molecular rotors are treated approximately as spherical tops.[14,27] For linear rotors, we employ the "integral approximation" for the sum of states given by Grice, Song, and Chesnavich.[29] The postcollision angular momentum distribution of the complex is treated in a statistical approximation as described elsewhere.[9] As also described in detail previously,[1,3,5,9,24] the model cross sections are convoluted over experimental translational and internal energy distributions, and then both channels are fit simultaneously by nonlinear least-squares regression to obtain ΔE_0 and $E_0(3b)$, where $\Delta E_0 = E_0(3b) - E_0(3a)$. Two additional adjustable parameters are N, which describes the energy transfer distribution in a modified line-of-centers collision model, and a single scaling factor σ_0 that is applied to both channels.[1,3,5,9] All calculations are performed with the CRUNCH data analysis and modeling program.[31]

The transition states are treated either as loose, orbiting transition states (OTS) or as tight, fixed transition states. The orbiting transition state is located variationally at the top of the centrifugal barrier on the ion−neutral potential energy surface for separating fragments. The long-range potential consists of the ion-induced-dipole potential and optionally the ion-permanent-dipole potential, treated here in a locked-dipole approximation.[30,32] The molecular parameters[17,20,33−37] used in the statistical rate calculations and thermal corrections are presented in Table 2. The loose transition states employ the vibrational and rotational constants of the product fragments. The tight TS parameters are assumed to be equal to those of the reactant complex ion with the vibrational mode corresponding to proton transfer removed as the reaction coordinate. Estimates for the anharmonicities associated with the complex ion are obtained

TABLE 2: Molecular Parameters for Statistical Rate Calculations

species	vibrational freq (cm^{-1})[a]	rotational consts (cm^{-1})	polarizability[b] (Å^3)	dipole moment[c] (D)
HS$^-$	2648 (53)[d]	9.39[d]		
HCN	743 (11), 2129 (12), 3442 (57)[e]	1.473[e]	2.59	2.985
HNC	477, 2029, 3652[f]	1.1521[f]	2.59	3.05
CN$^-$	2035 (14)[g]	1.875[g]		
H$_2$S	2722 (24), 1215 (5.7), 2733 (25)[h]	9.67, 4.72, 4.72[g]	3.78	0.978
HS$^-$···HCN[i]	147, 167, 180 (1.2),[j] 262, 967 (14), 1042 (15), 1955 (11), 2604 (43), 2619 (52)	9.42, 0.073, 0.072		

[a] Anharmonicities (cm^{-1}) given in parentheses. [b] Reference 36. [c] Reference 37. [d] Reference 35. [e] Reference 33. [f] Reference 20. [g] Reference 17. [h] Reference 34. [i] B3LYP/aug-cc-pVDZ. Anharmonicities estimated as described in text. [j] Proton-transfer reaction coordinate mode, removed to form a tight transition state for channel (3a).

TABLE 3: Theoretical Enthalpies at 0 K (kJ/mol)

method	$\Delta_{acid}H_0$(H$_2$S)	$\Delta_{acid}H_0$(HCN)	$\Delta_r H_0$(4)
B3LYP/aug-cc-pVDZ	1450.9	1449.4	1.5
B3LYP/aug-cc-pVTZ	1460.1	1459.0	1.1
B3LYP/aug-cc-pVQZ	1462.1	1459.7	2.4
CCSD(T)/aug-cc-pVTZ //B3LYP/aug-cc-pVTZ[a]	1465.6	1461.1	4.5
CCSD(T)/aug-cc-pVQZ //B3LYP/aug-cc-pVTZ[a]	1464.4	1461.2	3.2
CCSD(T)/aug-cc-pVQZ //CCSD(T)/aug-cc-pVTZ[a]	1464.4	1462.0	2.4
W1[b]	1465.0	1463.2	1.8 ± 1.2[c]
CBS-QB3[d]	1462.8	1461.0	1.8 ± 3.6[c]
CBS-Q[d]	1461.0	1460.5	0.5 ± 4.2[c]
G3(B3)[e]	1464.7	1464.8	−0.1 ± 4.1[c]
G3[e]	1464.4	1464.1	0.3 ± 4.2[c]
expt[f]	1464.92 ± 0.04	1462.3 ± 0.9	2.6 ± 0.9

[a] Vibrational zero-point energies calculated at the same level as geometries. [b] Reference 45. [c] Error limit is the reported mean absolute deviation of the compound method compared with experimental test sets. [d] References 46 and 47. [e] References 48 and 63. [f] Table 1.

by first correlating their normal modes with those of the products and then multiplying their frequencies with the anharmonicity-to-harmonic frequency ratio of the relevant product mode. The transitional mode frequencies are assumed to be harmonic. The anharmonicity for the reaction coordinate mode in the complex is calculated within the Morse oscillator approximation using the calculated frequency and the measured dissociation energy.

Computational Chemistry. Molecular structure calculations are performed using Gaussian 03.[38] For geometries and frequencies, density functional theory (DFT) is used with the hybrid Becke three-parameter exchange functional[39] with the Lee−Yang−Parr correlation functional (B3LYP).[40] For energy calculations, coupled-cluster theory with single and double excitations and perturbative treatment of triples [CCSD(T)][41] is also utilized. Dunning's augmented correlation-consistent polarized-valence basis sets are used, with double- (aug-cc-pVDZ), triple-(aug-cc-pVTZ), or quadruple-ζ (aug-cc-pVQZ) expansions.[42−44]

Theoretical Results

Gas-Phase Acidities. The 0 K gas-phase acidities of H$_2$S and HCN and the reaction enthalpy for reaction 4 calculated using several levels of theory and compound methods[45−48] are shown in Table 3. The results indicate that (a) for DFT a triple-ζ or larger basis set is required to obtain gas-phase acidities within 5 kJ/mol of the experimental values, (b) for CCSD(T) a large basis set and a geometry optimized at the CCSD(T) level is required to converge to values within the experimental uncertainties, and (c) all of the compound methods perform within their claimed accuracies. The W1 method agrees best with the experimental acidities. The calculated energies generally corroborate the literature thermochemical values.

Potential Energy Surface. Proton-transfer potential energy surfaces found using the intrinsic reaction coordinate method[49]

at the B3LYP/aug-cc-pVDZ level are presented in Figure 1a for reaction 4 and the corresponding reaction with the HNC isomer, plotted as a function of $\delta r = r(SH) - r(CH)$ and $\delta r = r(SH) - r(NH)$, respectively. The asymptotic energy for reaction 4 at this level of theory has a value of 1.5 kJ/mol after zero-point energy corrections, compared with the thermochemical value of 2.6 ± 0.9 kJ/mol. The geometries on the ground-state singlet surface are all planar (C_s symmetry). The global minimum of the potential energy surface is HS$^-$···HCN, an H-bonded complex between HS$^-$ and HCN with a separation of $r(S^-···H) = 2.178$ Å.

For the CN$^-$ + H$_2$S entrance channel of reaction 4, the dipole-aligned C_{2v} orientation is energetically favored asymptotically for separated fragments. As the two fragments approach, the H-bonding orientation is adopted via rotation of H$_2$S relative to CN$^-$. This reorientation occurs at intermediate range, $\delta r = -2.5$ to -1 Å, and proton transfer from H$_2$S to CN$^-$ occurs around $\delta r = 0$. There is no [HSH··CN$^-$] local minimum on this potential energy surface, only an inflection. Gronert and Kimura[50] found a true minimum for [HSH··CN$^-$], i.e., a double-well potential, using Moller−Plesset second-order perturbation (MP2) calculations with a 6-31+G(d,p) basis set. We could reproduce that result, but we find that the central barrier disappears with either larger basis sets or using DFT instead of MP2.

The HS$^-$···HCN minimum-energy complex separates to HS$^-$ + HCN products along a smooth surface with no reverse activation barriers. Dissociation through channel (3b) should therefore involve a loose transition state. The dissociation pathway back to CN$^-$ + H$_2$S also has no overall energy barrier, but (anticipating the experimental results below) it might be impeded by the requirement of proton transfer before ion−molecule separation along the dissociation coordinate.

The calculated [HS··H··NC]$^-$ isomeric potential energy surface (dashed line in Figure 1a) exhibits a double well-potential with a small potential energy barrier to proton transfer between S and N, which however is below the zero-point vibrational energy. The [HS$^-$··HNC] complex has a higher energy than the [HS$^-$··HCN] complex by about 32 kJ/mol. Although HSH··NC$^-$ is a true local minimum, the frequency for the mode corresponding to internal rotation of NC$^-$ is only 66 cm^{-1}, suggesting that the HSH··NC$^-$ complex could fairly easily isomerize to the lower energy HSH··CN$^-$ surface and proceed to the global HS$^-$···HCN minimum. Even in the unlikely event that some ions are trapped on this surface in the flow tube ion source, they would dissociate solely into CN$^-$ + H$_2$S near threshold, contrary to the experimental results that show a strong preference for the other product channel (see below).

Frequencies and Sums of States. To provide a more detailed view of the structural changes occurring during dissociation, we show in Figure 1b a correlation diagram of selected normal-mode frequencies along the reaction path for reaction 4. Strong

Collision-Induced Dissociation of HS⁻(HCN)

J. Phys. Chem. A, Vol. 110, No. 4, 2006 **1345**
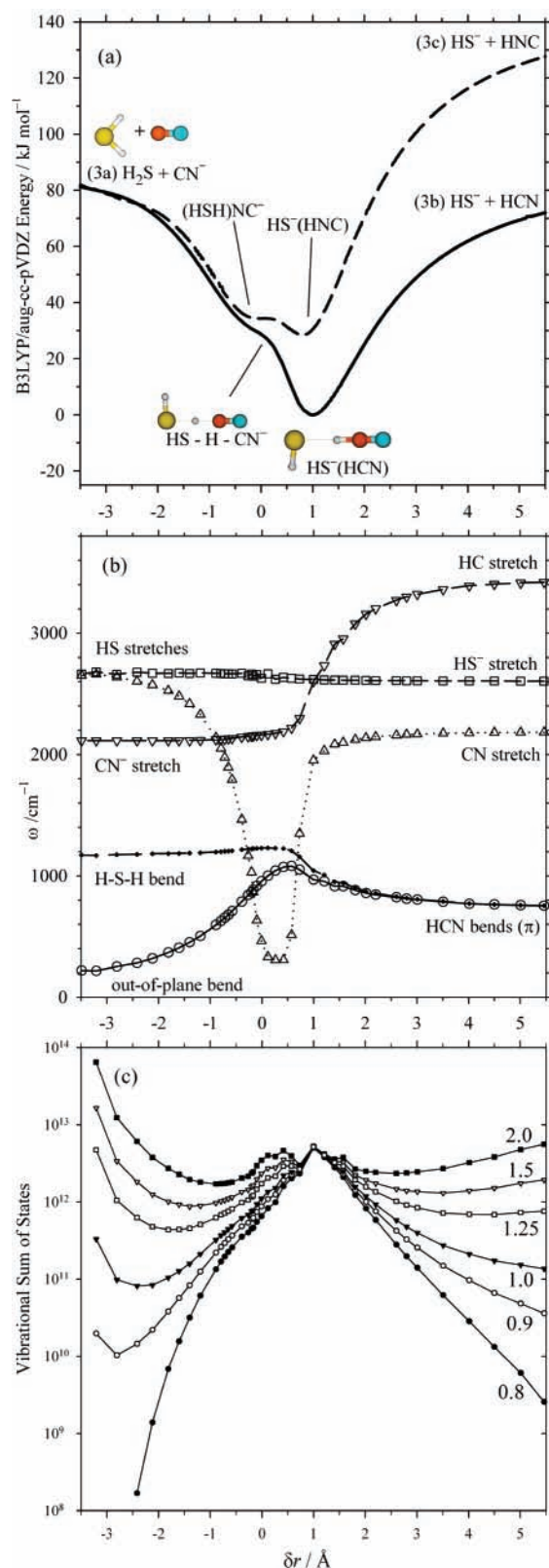
Figure 1. DFT calculations at the B3LYP/aug-cc-pVDZ level along the intrinsic reaction coordinate. (a) Potential energy surface for reaction 4 versus $\delta r = r(SH) - r(CH)$ (solid line) is shown, and the isomeric surface for HNC instead of HCN is also shown versus $\delta r = r(SH) - r(NH)$ (dashed line). (b) Correlation of selected normal-mode frequencies along the reaction path of reaction 4 is shown, excluding the reaction coordinate mode and three low-frequency transitional modes. (c) Vibrational sum of states along the reaction path in the harmonic oscillator approximation are shown. The curves are labeled by the total energy (potential energy plus vibrational energy) in electronvolts above the HS⁻(HCN) energy minimum.
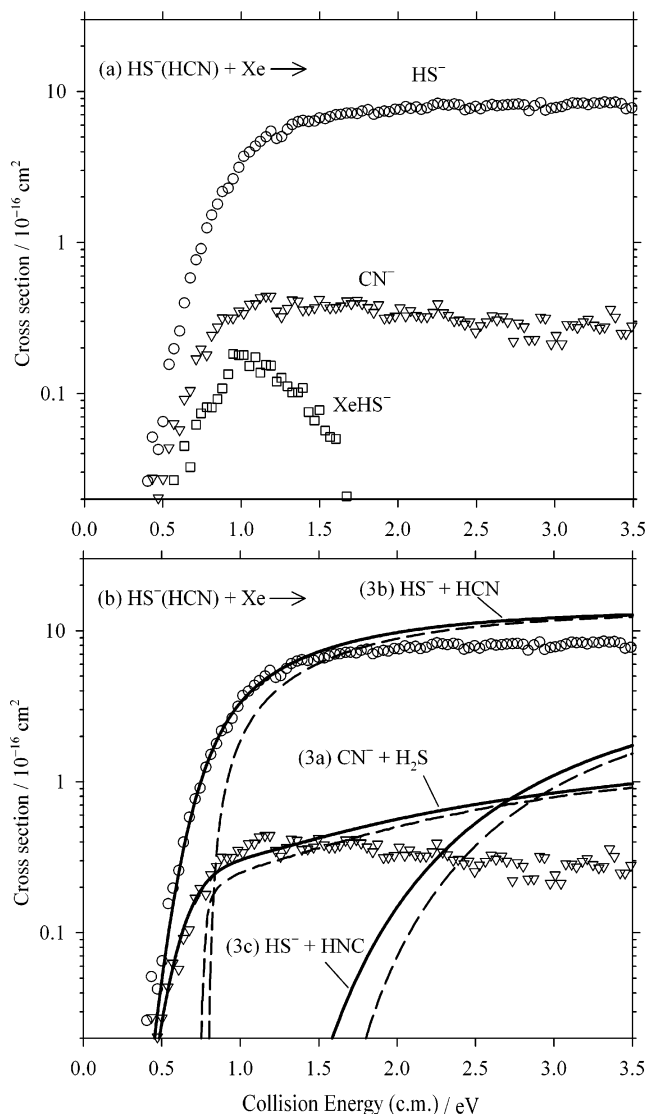
Figure 2. (a) Experimental cross sections for collision-induced dissociation of [HS⁻·HCN] with Xe. The ligand-exchange product Xe·HS⁻ is also shown. (b) Experimental (open symbols) and the convoluted (solid lines) and unconvoluted (dashed lines) model cross sections using the PST (scaled, dipole) model, fit to the threshold region for reactions 3a,b. The model cross section for the dissociation into HS⁻ + HNC products, reaction 3c, is also shown.

mode mixing occurs between H−CN stretch and HC−N stretch close to the complex geometry. Along the (3a) dissociation coordinate, the HC−N stretch character decreases and the H−CN stretch character increases. The HC−N stretch mode then couples with the H−S stretch in the proton-transfer region and evolves into the asymmetric H₂S stretch for channel (3a) products.

Figure 1c presents the vibrational sums of states along the reaction coordinate, calculated in the harmonic oscillator approximation for $J = 0$ and several total energies from 0.8 eV or 77 kJ/mol (just below threshold for channel 3a) to 2.0 eV or 193 kJ/mol. The minimum in the sum of states along each product channel represents the bottleneck for dissociation. This is intended as a qualitative picture—rotational states are not included, and the transitional modes would ideally be treated as hindered internal rotors instead of harmonic oscillators.

Experimental Results

TCID Cross Sections. Figure 2a shows representative experimental TCID cross sections for the dissociation of the

TABLE 4: Cross-Section Fits

model[a]	σ_0	N	ΔE_0 (eV)	E_0(3b) (eV)
RRKM	8.7	1.1	0.054 ± 0.014	0.84 ± 0.18
RRKM (dipole)	8.3	1.4	0.076 ± 0.014	0.83 ± 0.18
PST	7.1	1.0	0.052 ± 0.032	0.88 ± 0.33
PST (scaled)	8.6	1.5	0.066 ± 0.032	0.82 ± 0.33
PST (dipole)	7.0	1.0	0.049 ± 0.032	0.87 ± 0.33
PST (scaled, dipole)	8.4	1.4	0.062 ± 0.032	0.82 ± 0.33
"best" TCID value			0.062 ± 0.044	0.82 ± 0.40

[a] See text for explanations of various models.

complex into channels (3a) and (3b), along with the minor ligand exchange channel, reaction 3d. Both main product channels appear with apparent thresholds near 0.4 eV (cm). With increasing collision energy, the σ_{3b}/σ_{3a} ratio increases to about a factor of 50. This behavior indicates that channel (3a) is associated with a tighter transition state than channel (3b). The HS$^-$·Xe ion appears at the 0.4-eV threshold, peaks at 1.0 eV, and disappears by 2.0 eV, which is consistent with a ligand exchange process.[51] No CN$^-$·Xe product is observed. The observation of HS$^-$·Xe but not CN$^-$·Xe strongly corroborates the theoretical result that the reactant complex has the structure HS$^-$··HCN rather than either CN$^-$··H$_2$S or a strongly hydrogen-bonded intermediate structure with an equally shared proton. At 1.0 eV, the HS$^-$·Xe cross section is less than 10% of the HS$^-$ channel, with which it might compete. To determine whether the ligand-exchange channel affects the modeling of the main product channels, we tested replacement of the HS$^-$ cross section with the sum of the HS$^-$ and HS$^-$·Xe cross sections. This does not significantly affect any of the subsequent modeling parameters (described below). Therefore, this minor ligand-exchange channel can be ignored in the rest of the analysis. Its presence does indicate strong interactions between Xe and the cluster ions, which implies energy exchange among the internal degrees of freedom and lends credence to the use of statistical rate theory for the dissociation process.

Reaction 3c, formation of HS$^-$ + HNC, is a possible third dissociation channel for the complex. This channel, if present, would add to the HS$^-$ product from channel (3a) and would compete with CN$^-$ production. The asymptotic energy for the HS$^-$ + HNC products lies 5180 ± 700 cm^{-1} or 0.64 eV above the HS$^-$ + HCN asymptote.[52] This channel is considered theoretically below but cannot affect the fits to the cross sections of channels (3a) and (3b) near threshold.

Cross-Section Models and Threshold Fits. Several alternatives in application of the statistical rate theory models are described in this section, with results summarized in Table 4. The deviations among these models are minor and all of the models give threshold-region fits similar in quality to the "PST (scaled, dipole)" model shown in Figure 2b and described in more detail below. The adjustable parameters in Table 4 for RRKM theory and PST models are obtained from fits over the collision energy range 0−1.5 eV (cm), i.e., below the region where reaction 3c could influence the results. The uncertainties in ΔE_0 and E_0(3b) are determined as root-sum-of-squares of (a) the uncertainties arising from the ion energy determination (± 0.05 eV lab), (b) the statistical uncertainty in the least-squares fit to the data, (c) a range of reactant ion temperatures from 200 to 400 K, (d) the estimated standard deviation from fits to multiple sets of data, and (e) the uncertainty from the fitting parameters determined by scaling the vibrational modes by $\pm 20\%$, scaling only the transitional modes by $\pm 20\%$, scaling the reaction degeneracy for both channels together by a factor of 2, varying the reaction degeneracy in opposite directions for the two channels by factors of 2, and fitting various energy
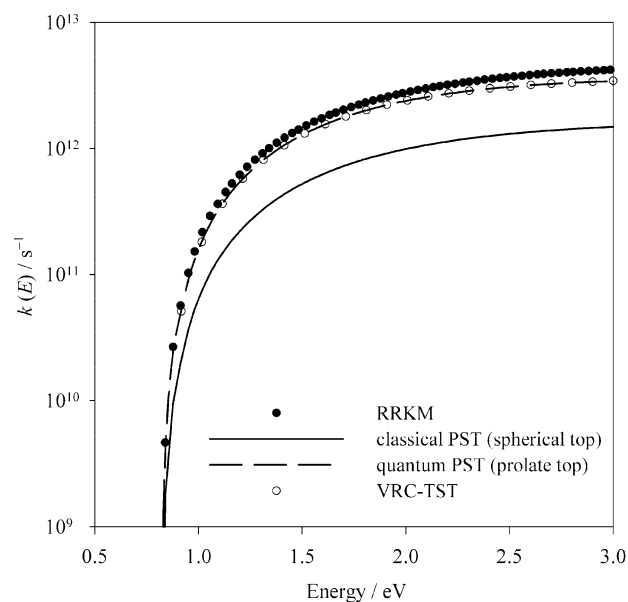
Figure 3. Statistical unimolecular dissociation rates, $k(E^*,J)$, for reaction 3b plotted versus the total energy E^* at $J = 46$. Shown are the results of RRKM theory, classical PST with the spherical rotor approximation, quantum PST, and VRC-TST, as described in the text.

ranges with upper limits from 1 to 2 eV. The reported error bars represent our estimate of ± 2 combined standard uncertainties.[53]

Attempts to model the cross sections for the two primary product channels (3a) and (3b) using either both loose, orbiting transition states or both tight, fixed transition states fail. Rather, the dominant HS$^-$ + HCN product channel must be modeled with a loose transition state and the smaller H$_2$S + CN$^-$ channel with a tight transition state. The extreme behavior of this system, with nearly identical threshold energies but very different magnitudes for the two main channels, makes it difficult to fit but that also constrains the range of the transition state models that can be used. The unconvoluted model (for zero internal energy and no translational energy distribution), dashed lines in Figure 2b, shows that the tight channel (3a) has the lower threshold energy. But at a slightly higher energy, the loose channel (3b) becomes accessible and rapidly overtakes and competitively suppresses channel (3a). Channel (3b) is best fit with the losest reasonable transition state, namely an orbiting transition state at the centrifugal barrier. For the tight channel (3a), we tested reducing the transitional mode frequencies but found that the calculated frequencies for the complex gave the best fit; that is, the tightest reasonable frequency parameters are required.

We apply both RRKM theory and classical PST for the statistical unimolecular dissociation rate constant. To evaluate the approximations and the implementations of these models in CRUNCH,[31] we compared the energy-dependent rate constants, $k(E)$, for RRKM theory and classical PST to each other and to quantum PST and variable reaction coordinate transition state theory (VRC-TST) calculated using the VARIFLEX program of Klippenstein et al.[54] For the tight TS for channel (3a), the results are essentially identical for RRKM theory, classical PST, and quantum TST. Some differences are found for the orbiting transition state for channel (3b), however, as shown in Figure 3 for $J = 46$, which is the average J for the statistical angular momentum distribution[9] at threshold. (This value of J is chosen to illustrate the effects; similar results are found for other J values.) The RRKM theory and VRC-TST rates agree with each other within 10% at higher energies and are in perfect agreement

near the threshold for this J. This indicates that (a) the position and the height of the centrifugal barrier are calculated to be similar by both methods and (b) for this J the rates are insensitive to the inclusion and treatment of permanent-dipole potential. In contrast, the quantum PST rate curves calculated using VARIFLEX[54] and classical PST rate curves calculated in CRUNCH[31] using the code adapted from Chesnavich and Bowers[14] are found to differ by a factor of about 2.4 for various energies and J values. We traced this deviation to be almost entirely the result of the use of the spherical rotor approximation in this implementation of classical PST.[14] When spherical rotational constants are used as input parameters in variflex, the quantum PST rates agree well with the classical PST rates. Chesnavich and Bowers[14] found that the error introduced by using the spherical rotor approximation was small for the oblate and prolate systems they tested. However, for this reaction the extreme rotational asymmetry of the near-prolate [HS⁻·HCN] complex ($A = 9.42$ cm⁻¹, $B = 0.073$ cm⁻¹, $C = 0.072$ cm⁻¹) makes the spherical approximation (with a geometric mean rotational constant of 0.367 cm⁻¹) problematic. Because the shapes of the $k(E,J)$ curves are very similar for classical PST with the spherical approximation and for quantum PST using symmetric top rotors, we applied a scaling factor of 2.4 to the PST rates for channel (3b). Both unscaled and scaled models are given in Table 4.

The rotational symmetry numbers for the energized molecule (EM) and the TS for product channel (3b), HS⁻ + HCN, are both $\sigma = 1$, because they have only a plane of symmetry (C_s). Therefore, the reaction degeneracy is $s_{3b} = \sigma_{EM}/\sigma_{3b} = 1$. For product channel (3a), the tight transition state could have either $\sigma_{TS} = 1$ (hydrogen-bonded C_s configuration) or $\sigma_{3a} = 2$ (the dipole-aligned C_{2v} configuration at longer range). The fits calculated with $\sigma_{3a} = 1$ were slightly better, while using $\sigma_{3a} = 2$ increased ΔE_0 about 5 meV for RRKM or by 50 meV for PST. For consistency with the theoretical potential energy surface and for better fit quality, we set $\sigma_{3a} = 1$. The small variations of the results with respect to the symmetry parameter choices are taken into account in the error analysis as described above.

Because channel (3a) goes through the proton-transfer region, which apparently results in the tight transition state, we also tried modeling this channel with a transition-state switching model,[26] for which the sum of states at each E^* and J is replaced by the minimum sum of states for an inner tight TS versus an outer orbiting TS. However, when the parameters for this model are optimized, the energy of the inner tight TS tended toward the dissociation energy and the orbiting TS never limited the sum of states. That is, the results of the transition-state switching model were experimentally indistinguishable from using a tight TS alone. A fully variational transition state theory method on a multidimensional potential energy surface would be required to elucidate the true nature of the bottleneck on this surface, but empirically a tight transition state is required to model the data for channel (3a).

As summarized in Table 4, all alternative models give very similar results for ΔE_0 and E_0(3b). The nominal values for ΔE_0 vary over a small range of 0.049−0.076 eV. Curiously, the inclusion of the locked dipole slightly increases ΔE_0 for RRKM but decreases it very slightly for PST, but the effect is not large for either. In general, the small deviations in ΔE_0 among the various models are barely significant statistically and hence cannot be definitively interpreted in terms of physical effects. The estimated error bars for the PST models are larger than for RRKM because the former are more sensitive to input frequen-

cies, symmetry numbers, and reactant temperature. For the "best" TCID value of ΔE_0, we select the scaled classical PST model with inclusion of the permanent dipole because PST properly conserves total angular momentum and the scaling factor compensates for the error from using spherical rotational constants. This fit for channels (3a) and (3b) is shown in Figure 2b. The uncertainty limits for the best value are increased to account for the range of values from various statistical rate models, yielding a final result of $\Delta E_0 = 0.062 \pm 0.044$ eV.

Figure 2b also displays the model cross section for channel (3c), formation of HS⁻ + HNC, calculated using the literature energy[52] relative to product channel (3a) and a loose transition state model. A loose transition state gives an upper limit for the cross section. Adding this model cross section into the HS⁻ + HCN channel would have no effect in the threshold region below 1.5 eV, where the data for channels (3a) and (3b) are fit. However, the calculated cross section for channel (3c) is similar in magnitude to channel (3b) at higher energies.

Discussion

Tight vs Loose Transition States. The TCID branching ratios for channels (3a) and (3b) clearly indicate the presence of a constraint toward dissociation through the CN⁻ + H₂S channel. That is, (3a) has a tight transition state and (3b) has a loose transition state. The constraint for channel (3a) is not obvious on the calculated potential energy surface in Figure 1a, which exhibits no potential energy barrier along the reaction path, only an inflection in the proton-transfer region. The frequency correlations in Figure 1b do suggest a difference between the two dissociation pathways. From the minimum-energy HS⁻···HCN complex at about $\delta r = 1$, the vibrational frequencies evolve smoothly to HS⁻ + HCN product frequencies, channel (3b). In contrast, for channel (3a) to CN⁻ + H₂S, the frequencies go through wide swings. This behavior indicates strong curvature along the reaction coordinate, which suggests that dynamic constraints could also be operative in the dissociation process for (3a).

Another view of the transition state behavior along the reaction coordinate may be gained by the plot of the vibrational sums of states shown in Figure 1c. For both reaction channels, the minimum in the sum of states (numerator in the statistical rate expression of eq 5) moves from long-range (indicative of a loose transition state) inward toward the minimum in the potential energy surface (indicative of a tighter transition state) as the energy increases. This tightening of the transition state region is more pronounced and occurs at lower energies for channel (3a) than for channel (3b). This analysis implies that a true microcanonical variational transition state theory would be ideally required to provide the best statistical model of the dissociation process, especially at higher energies. Empirically, however, we find that only the tight/loose combination of transition state parameters is able to reproduce the data near threshold.

Unsymmetrical Hydrogen Bonding in the Complex. Despite the nearly identical gas-phase acidities of H₂S and HCN, the hydrogen bonding in the proton-bound dimer anion [HS·H·CN] ⁻ is clearly unsymmetrical, defined as having unequal well depths for the two structures of the complex.[55] Both theoretical calculations and the experiments show that the complex has the structure HS⁻···HCN. The observations of (1) the HS⁻·Xe ligand-exchange product but not CN⁻·Xe and (2) the loose transition state for HS⁻ + HCN but tight transition state for CN⁻···H₂S together experimentally confirm the theoretical prediction of the HS⁻···HCN structure for the complex

(Figure 1a). The calculated energy of the $CN^-\cdots H_2S$ hydrogen-bonded structure, which is just an inflection point and not a local minimum of the PES, is about 32 kJ/mol higher than $HS^-\cdots HCN$, compared with the asymptotic acidity difference between H_2S and HCN of about 3 kJ/mol.

The reasons for the strongly unsymmetrical hydrogen bonding in the complex may be understood in terms of the electronic properties of the anions. Gronert and co-workers[50,56] have theoretically examined proton-bound anionic complexes for a variety of second- and third-period hydrides. The position of the transition state for proton transfer within the complex depends more on the proton donor/acceptor properties of the two acids than on the asymptotic energetics of the proton-transfer reaction.[50] The complexation energy is largest when the proton donor is a strongly electronegative element. As carbon is not strongly electronegative, carbon acids are known to behave differently and have weaker hydrogen bonding than "normal" nitrogen or oxygen acids.[57,58] However, HCN is the most "normal" carbon acid in solution[59] and is more akin to hydrogen halides because of the high electrophilicity of the CN group.[60] CN is more electronegative than HS: EA(CN) = 3.86 eV compared with EA(HS) = 2.31 eV (Table 1). Furthermore, second-period acids such as HCN are better hydrogen donors than third-period acids such as H_2S.[50] These factors favor the $HS^-\cdots HCN$ structure over $CN^-\cdots H_2S$. Furthermore, the $HS^-\cdots HCN$ structure is favored by the much larger dipole moment of HCN compared with H_2S (Table 2). The dipole of HCN is aligned toward the charge center in $HS^-\cdots HCN$, but the dipole of H_2S cannot be perfectly aligned in $CN^-\cdots H_2S$ while also maintaining an optimal near-linear N–H–S hydrogen bond. Solution phase proton exchange kinetic studies[59] show that the rate of proton removal from HCN by a sulfur base (RS^-) is several orders of magnitude slower than for nitrogen or oxygen bases. This has been attributed to the stronger proton donor properties of HCN compared with RSH, which stabilizes the $[RS^-\cdots HCN]$ complexes.

Higher Energy Behavior. Channel (3c), formation of HS^- + HNC, yields the same product ion mass as channel (3a), HS^- + HCN. The model cross sections in Figure 2b show that channel (3c) would have only a minor effect on the much larger channel (3a). However, channel (3c) is comparable in magnitude to channel (3b), CN^- + H_2S, and it appears in the higher-energy region where the experimental cross section for (3b) declines. That behavior suggests that there could be a competition between (3b) and (3c), counter to the assumption of the statistical model that all three dissociation channels arise from a common intermediate. A possible mechanism for such a competition is a two-step process:

$$[HS^-\cdots HCN] + Xe \rightarrow HS^- + HCN + Xe$$

$$\rightarrow [CN^-\cdots H_2S]^* + Xe$$

$$[CN^-\cdots H_2S]^* \rightarrow CN^- + H_2S$$

$$\rightarrow HS^- + HNC$$
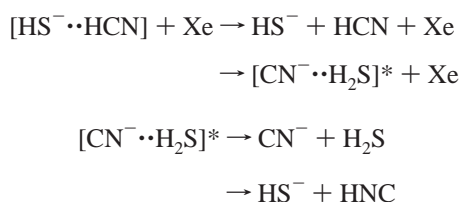
That is, the bottleneck for both processes (3b) and (3c) is the internal proton transfer to form the $[CN^-\cdots H_2S]^*$ intermediate, which can then either dissociate into CN^- + H_2S or else undergo another internal proton transfer with the nitrogen end of CN^- to form HS^- + HNC. Modeling this mechanism is beyond the scope of this work, but it does provide a speculative reason for the observed decline in the CN^- cross section at high energy and it is consistent with the tight transition state for channel (3b).

TABLE 5: Thermochemical Results

method	$\Delta_r H_0$ (kJ/mol)	$\Delta_r G_{298}$ (kJ/mol)
thermochem cycle[a]	2.6 ± 0.9	6.2 ± 0.9^b
equilibrium[c]	3.2 ± 0.4^b	6.7 ± 0.4
TCID (this work)	6.0 ± 4.3	9.5 ± 4.3^b

[a] Table 1. [b] Thermal entropy and enthalpy corrections calculated in the rigid rotor, harmonic oscillator approximation using B3LYP/aug-cc-pVTZ geometries and frequencies. [c] Reference 61.

Thermochemical Results. The enthalpies and Gibbs energies for reaction 4 are summarized in Table 5. The "best" TCID value for the endoergicity of reaction 4, $\Delta E_0 = 6.0 \pm 4.3$ kJ/mol, agrees within its uncertainty with the literature thermochemical value of $\Delta_r H_0(4) = 2.6 \pm 0.9$ kJ/mol (Table 1). The latter value agrees well with an independent ion-cyclotron resonance equilibrium study of reaction 4,[61] which gives $\Delta_r H_0$-(4) = 3.2 ± 0.4 kJ/mol after thermal corrections. However, RRKM fits on the TCID cross sections performed by fixing ΔE_0 at the literature value of 2.6 kJ/mol and relaxing the other three adjustable parameters $[\sigma_0, N, \text{ and } E_0(3a)]$ were unsatisfactory. The shift in the threshold of the model CN^- cross section could not be compensated by reasonable adjustments to the TS parameters. That implies that although the error is within known random and modeling uncertainties, the small remaining deviation may be systematic (either experimental or in the statistical models for this work or as an outside possibility in the literature thermochemistry) rather than simply due to random error. Figure 1c suggests that the statistical rate theory might be improved using a true variational description of the transition states as a function of energy rather than the limiting cases of loose (orbiting) and tight (fixed) transition states. Theoretical dynamics studies could probe whether there is also a nonstatistical component to the TCID process for reaction 3a, but that is beyond the scope of this work.

Treating the gas-phase acidity of H_2S, $\Delta_{acid} H_0(H_2S) = 1464.92 \pm 0.04$ kJ/mol, as the "known" because it is more precise than $\Delta_{acid} H_0$(HCN), we can derive $\Delta_{acid} H_0$ (HCN) = 1459 ± 4 kJ/mol as the "best" TCID value from this work. This agrees with the literature value of $\Delta_{acid} H_0$(HCN) = 1462.3 ± 0.9 kJ/mol within the uncertainty limits, as expected from the discussion above.

The measured complexation energy of $HS^-\cdots HCN$ relative to the lower energy products CN^- + H_2S is $E_0(3a) = E_0$ (3b) $- \Delta E_0 = 0.76 \pm 0.40$ eV or 73 ± 39 kJ/mol. This agrees well with the more precise complexation energy of 79 ± 4 kJ/mol reported for "$CN^-\cdots H_2S$" from ligand-exchange equilibria in high-pressure mass spectrometry experiments.[62] However, the present work shows that the actual structure of the complex ion is $HS^-\cdots HCN$.

Conclusion

The cross sections for the collision-induced dissociation of $[HS^-\cdots HCN]$ proton-bound complex to CN^- + H_2S and HS^- + HCN have been measured using the competitive TCID method. The results indicate that the CN^- + H_2S product channel passes through a tight transition state and the HS^- + HCN channel is associated with a loose transition state. The calculated potential energy surface has a single minimum and shows no barrier along the dissociation path for either channel. The calculations confirm that the complex ion has the unsymmetrical form $HS^-\cdots HCN$, i.e., a hydrogen bonded complex between HS^- and HCN. This complex can fall apart facilely to HS^- + HCN (the "loose" channel) but must pass through a proton-transfer region to reach CN^- + H_2S products (the "tight"

channel). The requirement for the proton transfer evidently results in a bottleneck despite the absence of a potential energy barrier on the surface. Normal mode calculations show that there is strong curvature along the reaction path toward the $CN^- + H_2S$ channel, consistent with the tight transition state for that channel.

The product branching ratios have been modeled both using RRKM theory and phase space theory. Both treatments give similar reaction thermochemistry. Treatment of the permanent dipole of HCN in the orbiting transition state either in a locked-dipole approximation or by neglecting the dipole entirely has only minor effects on the resulting energy differences. This lack of sensitivity to modeling parameters reflects the robustness of the competitive TCID method.

References and Notes

(1) Rodgers, M. T.; Armentrout, P. B. *J. Chem. Phys.* **1998**, *109*, 1787.
(2) Ervin, K. M. *Chem. Rev.* **2001**, *101*, 391. Erratum. *Chem. Rev.* **2002**, *102*, 855.
(3) DeTuri, V. F.; Ervin, K. M. *J. Phys. Chem. A* **1999**, *103*, 6911.
(4) Shi, Y.; Ervin, K. M. *Chem. Phys. Lett.* **2000**, *318*, 149.
(5) Angel, L. A.; Ervin, K. M. *J. Phys. Chem. A* **2004**, *108*, 8345.
(6) Muntean, F.; Armentrout, P. B. *J. Phys. Chem. A* **2003**, *107*, 7413.
(7) Ye, S. J.; Moision, R. M.; Armentrout, P. B. *Int. J. Mass Spectrom.* **2005**, *240*, 233.
(8) Liu, X.; Gross, M. L.; Wenthold, P. G. *J. Phys. Chem. A* **2005**, *109*, 2183.
(9) Rodgers, M. T.; Ervin, K. M.; Armentrout, P. B. *J. Chem. Phys.* **1997**, *106*, 4499.
(10) Muntean, F.; Armentrout, P. B. *J. Chem. Phys.* **2001**, *115*, 1213.
(11) Gilbert, R. G.; Smith, S. C. *Theory of Unimolecular and Recombination Reactions*; Blackwell Scientific: Boston, MA, 1990.
(12) Baer, T.; Hase, W. L. *Unimolecular Reaction Dynamics: Theory and Experiments*; Oxford University Press: New York, 1996.
(13) Pechukas, P.; Light, J. C. *J. Chem. Phys.* **1965**, *42*, 3281.
(14) Chesnavich, W. J.; Bowers, M. T. *J. Chem. Phys.* **1977**, *66*, 2306.
(15) Larson, D. J.; Edge, C. J.; Elmquist, R. E.; Mansour, N. B.; Trainham, R. *Phys. Scr. T* **1988**, *22*, 183.
(16) Shiell, R. C.; Hu, X. K.; Hu, Q. J.; Hepburn, J. W. *J. Phys. Chem. A* **2000**, *104*, 4339.
(17) Bradforth, S.; Kim, E.; Arnold, D.; Neumark, D. *J. Chem. Phys.* **1993**, *98*, 800.
(18) Morley, G. P.; Lambert, I. R.; Mordaunt, D. H.; Wilson, S. H. S.; Ashfold, M. N. R.; Dixon, R. N.; Western, C. M. *J. Chem. Soc. Faraday Trans.* **1993**, *89*, 3865.
(19) Cook, P. A.; Langford, S. R.; Ashfold, M. N. R.; Dixon, R. N. *J. Chem. Phys.* **2000**, *113*, 994.
(20) Gurvich, L. V.; Veyts, I. V.; Alcock, C. B. *Thermodynamic Properties of Individual Substances*, 4th ed.; Hemisphere Publishing Corp.: New York, 1989; Vol. 1 (Elements O, H (D, T), F, Cl, Br, I, He, Ne, Ar, Kr, Xe, Rn, S, N, P and Their Compounds), Parts 1 and 2.
(21) DeTuri, V. F.; Hintz, P. A.; Ervin, K. M. *J. Phys. Chem. A* **1997**, *101*, 5969.
(22) Spasov, V. A.; Ervin, K. M. *J. Chem. Phys.* **1998**, *109*, 5344.
(23) Angel, L. A.; Ervin, K. M. *J. Am. Chem. Soc.* **2003**, *125*, 1014.
(24) Ervin, K. M.; Armentrout, P. B. *J. Chem. Phys.* **1985**, *83*, 166.
(25) Chesnavich, W. J.; Bowers, M. T. In *Gas-Phase Ion Chemistry*; Bowers, M. T., Ed.; Academic: New York, 1979; p 119.
(26) Chesnavich, W. J.; Bass, L.; Su, T.; Bowers, M. T. *J. Chem. Phys.* **1981**, *74*, 2228.
(27) Chesnavich, W. J.; Bowers, M. T. *Prog. React. Kinet.* **1982**, *11*, 137.

(28) Webb, D. A.; Chesnavich, W. J. *J. Phys. Chem.* **1983**, *87*, 3791.
(29) Grice, M. E.; Song, K.; Chesnavich, W. J. *J. Phys. Chem.* **1986**, *90*, 3503.
(30) Bass, L. M.; Bowers, M. T. *J. Chem. Phys.* **1987**, *86*, 2611.
(31) Armentrout, P. B.; Ervin, K. M. CRUNCH, Fortran program, version 5.0, 2003.
(32) Iceman, C.; Armentrout, P. B. *Int. J. Mass Spectrom.* **2003**, *222*, 329.
(33) Dykstra, C. E.; Secrest, D. *J. Chem. Phys.* **1981**, *75*, 3967.
(34) Topper, R. Q.; Zhang, Q.; Liu, Y.-P.; Truhlar, D. G. *J. Chem. Phys.* **1993**, *98*, 4991.
(35) Breyer, F.; Frey, P.; Hotop, H. *Z. Phys. A* **1981**, *300*, 7.
(36) Lide, D. R., Jr. Dipole Moments of Molecules in the Gas Phase. In *Handbook of Chemistry and Physics*; Lide, D. R., Ed.; CRC Press: Boca Raton, FL, 1996; p 9.
(37) Miller, T. M. Atomic and Molecular Polarizabilities. In *Handbook of Chemistry and Physics*; Lide, D. R., Ed.; CRC Press: Boca Raton, FL, 1996; p 10199.
(38) Frisch, M. J.; Trucks, G. W.; Schlegel, H. B.; Scuseria, G. E.; Robb, M. A.; Cheeseman, J. R.; Montgomery, J., J. A.; Vreven, T.; Kudin, K. N.; Burant, J. C.; Millam, J. M.; Iyengar, S. S.; Tomasi, J.; Barone, V.; Mennucci, B.; Cossi, M.; Scalmani, G.; Rega, N.; Petersson, G. A.; Nakatsuji, H.; Hada, M.; Ehara, M.; Toyota, K.; Fukuda, R.; Hasegawa, J.; Ishida, M.; Nakajima, T.; Honda, Y.; Kitao, O.; Nakai, H.; Klene, M.; Li, X.; Knox, J. E.; Hratchian, H. P.; Cross, J. B.; Bakken, V.; Adamo, C.; Jaramillo, J.; Gomperts, R.; Stratmann, R. E.; Yazyev, O.; Austin, A. J.; Cammi, R.; Pomelli, C.; Ochterski, J. W.; Ayala, P. Y.; Morokuma, K.; Voth, G. A.; Salvador, P.; Dannenberg, J. J.; Zakrzewski, V. G.; Dapprich, S.; Daniels, A. D.; Strain, M. C.; Farkas, O.; Malick, D. K.; Rabuck, A. D.; Raghavachari, K.; Foresman, J. B.; Ortiz, J. V.; Cui, Q.; Baboul, A. G.; Clifford, S.; Cioslowski, J.; Stefanov, B. B.; Liu, G.; Liashenko, A.; Piskorz, P.; Komaromi, I.; Martin, R. L.; Fox, D. J.; Keith, T.; Al-Laham, M. A.; Peng, C. Y.; Nanayakkara, A.; Challacombe, M.; Gill, P. M. W.; Johnson, B.; Chen, W.; Wong, M. W.; Gonzalez, C.; Pople, J. A. *Gaussian 03*, revision C.02; Gaussian, Inc.: Wallingford, CT, 2004.
(39) Becke, A. J. *Chem. Phys.* **1993**, *98*, 5648.
(40) Lee, C.; Yang, W.; Parr, R. G. *Phys. Rev. B* **1988**, *37*, 785.
(41) Pople, J. A.; Head-Gordon, M.; Raghavachari, K. *J. Chem. Phys.* **1987**, *87*, 5968.
(42) Dunning, T. H., Jr. *J. Chem. Phys.* **1989**, *90*, 1007.
(43) Kendall, R. A.; Dunning, T. H., Jr.; Harrison, R. J. *J. Chem. Phys.* **1992**, *96*, 6792.
(44) Woon, D. E.; Dunning, T. H., Jr. *J. Chem. Phys.* **1993**, *98*, 1358.
(45) Martin, J. M. L.; de Oliveira, G. *J. Chem. Phys.* **1999**, *111*, 1843.
(46) Ochterski, J. W.; Petersson, G. A.; Montgomery, J. A., Jr. *J. Chem. Phys.* **1996**, *104*, 2598.
(47) Montgomery, J. A., Jr.; Frisch, M. J.; Ochterski, J. W.; Petersson, G. A. *J. Chem. Phys.* **1999**, *110*, 2822.
(48) Curtiss, L. A.; Raghavachari, K.; Redfern, P. C.; Rassolov, V.; Pople, J. A. *J. Chem. Phys.* **1998**, *109*, 7764. (Supporting Information at http://chemistry.anl.gov/compmat/comptherm.htm.)
(49) Gonzalez, C.; Schlegel, H. B. *J. Phys. Chem.* **1990**, *94*, 5523.
(50) Gronert, S.; Kimura, C. *J. Phys. Chem. A* **2003**, *107*, 8932.
(51) Rodgers, M. T.; Armentrout, P. B. *J. Phys. Chem. A* **1997**, *101*, 2614.
(52) Barber, R. J.; Harris, G. J.; Tennyson, J. J. *J. Chem. Phys.* **2002**, *117*, 11239.
(53) Taylor, B. N.; Kuyatt, C. *Guidelines for Evaluating and Expressing the Uncertainty of NIST Measurement Results*; NIST Technical Note 1297; National Institute of Standards and Technology: Washington, DC, 1994. (http://physics.nist.gov/Document/tn1297.pdf, accessed 12/1/2004.)
(54) Klippenstein, S. J.; Wagner, A.; Roberstson, S.; Dunbar, R.; Wardlaw, D. M. VARIFLEX, version 1.0, 1999.
(55) Vinogradov, S. N.; Linnell, R. H. *Hydrogen Bonding*; Van Nostrand Reinhold: New York, 1971.
(56) Gronert, S. *J. Am. Chem. Soc.* **1993**, *115*, 10258.
(57) Bell, R. P. *The Proton in Chemistry*, 2nd ed.; Cornell University Press: Ithaca, NY, 1973.
(58) Peräkylä, M. *J. Phys. Chem.* **1996**, *100*, 3441.
(59) Bednar, R. A.; Jencks, W. P. *J. Am. Chem. Soc.* **1985**, *107*, 7117.
(60) Parr, R. G.; von Szentpály, L.; Liu, S. *J. Am. Chem. Soc.* **1999**, *121*, 1922.
(61) Betowski, D.; Mackay, G.; Payzant, J.; Bohme, D. *Can. J. Chem.* **1975**, *53*, 2365.
(62) Meot-Ner (Mautner), M. *J. Am. Chem. Soc.* **1988**, *110*, 3854.
(63) Baboul, A. G.; Curtiss, L. A.; Redfern, P. C.; Raghavachari, K. *J. Chem. Phys.* **1999**, *110*, 7650.